Direct Growth of Al Nanowire Arrays: Thermal Expansion and Field Emission Properties

Liang Li,*,† Xijin Xu,‡ Hanguan Chew,§ Xiaohu Huang,† Xincun Dou,† Shusheng Pan,† Guanghai Li,† and Lide Zhang†

Anhui Key Laboratory of Nanomaterials and Nanotechnology, Institute of Solid State Physics, Chinese Academy of Science, Hefei 230031, China, Nanoelectronics Lab, School of Electrical and Electronic Engineering, Nanyang Technological University, Singapore, and Chartered Semiconductor Manufacturing Limited, 60 Woodlands Industrial Park D, Street 2, Singapore

Received: October 23, 2007; In Final Form: February 1, 2008

The Al nanowire arrays were directly deposited on the Si substrates by a facile electron-beam evaporation technique, oblique angle deposition. This process was accomplished by tilting the Si substrates and adjusting the incident angle of evaporated Al vapor flux from the normal of the substrates at 87°. X-ray diffraction, scanning electron microscopy, and transmission electron microscopy observations indicate that large-area and single-crystalline Al nanowire arrays are effectively fabricated. In situ high-temperature X-ray diffraction measurements show that Al nanowires have a smaller lattice constant and smaller thermal expansion coefficient compared with the Al film. The thermal expansion mechanism was discussed in detail. Our field emission results show that the Al nanowires might be potential field emitters in the future nanodevices.

1. Introduction

Metal nanowires are interesting from a fundamental as well as a technological point of view, and they are expected to play an important role as components or interconnects in fabricating nanoscale devices.[1] Assembly of high-density metallic nanowires, particularly nanowire arrays, can be usually obtained by electrodeposition of the species into the nanochannels of a porous template such as anodic alumina and polymeric ion-track membrane.[2−5] These porous templates can support nanowires in three-dimensional space and facilitate depositing electrical contacts on the top of nanowires, and thus conveniently studying electrical, magnetic, and sensing properties.

Oblique angle deposition (OAD), developed by Robbie and Brett,[6] exploits atomic shadowing effects during line-of-sight physical vapor deposition to create arrays of uniquely shaped nanostructures with a variety of shapes, diameters, separations, heights, and topographies. During deposition, the substrate is tilted with an angle between the incoming vapor from the source and the surface normal of the substrate. This angle is usually set between 70° and 90° (oblique angle). Because of a shadowing effect, quasi-aligned nanowire arrays will self-assemble on the substrate. The two main competing factors that control the growth are the shadowing effect and surface diffusion. The distance and height of the nanowires can be controlled by the incident angle and deposition time; thus, nanostructures with a desired density and surface roughness can be achieved. Some of the advantages of the OAD are as follows: no templates are needed, no high temperatures are required, and no harmful chemical residues are involved. Recently, efforts have been devoted to manipulating the various shaped nanostructures such as zigzags, pillars, spirals, slanted posts, columns, with potential applications as magnetic storage media, sensors, actuators, and field emitters.[7−11]

In the past few years, there are numerous studies on structure and physical properties of nanowires; however, the thermal expansion and field emission knowledge of metallic nanowires is quite limited up to now.[12−14] As we all know, the thermal stability of nanostructures is of critical importance for their implementation as building blocks in nanoscale electronic and photonic devices. Recently, our group first reported the observation of the unique thermal expansion behavior of some metallic nanowires embedded in the anodic alumina membranes (AAM).[15−17] At the same time, at the tip of such conductive nanostructures, field electron emission by tunneling can occur at a few V/μm due to local electrical field enhancement. Furthermore, these nanostructures are potential cold electron sources in vacuum nanoelectronics because no high temperatures are required.[18−21] Among these studies, one inevitable problem is how to exclude the effect of the surrounding AAM medium and exactly extract the intrinsic properties of nanowires.

In this paper, we employed OAD to fabricate template-free Al nanowire arrays and measured the thermal expansion of the Al nanowires using in situ high-resolution X-ray diffraction with elevating temperature. The direct growth of quasi-aligned Al nanowires on the Si substrates makes the products potential candidates for field-emission performance, but has not been reported to date and is also the subject of this work. The Al nanowire was selected as an example due to its high electrical conductivity and applications in interconnect devices.

2. Experimental Section

The samples were fabricated in a high-vacuum electron beam evaporation system with a background pressure of 4×10^{-7} Torr. The Si substrates were cleaned by the standard RCA (Radio Corporation of America) I and II process prior to every deposition. The incident angle of vapor flux with respect to the substrate normal was fixed at 87°. The distance between the evaporation source and the substrate was about 20 cm. During the deposition, the pressure was about 4×10^{-6} Torr, the growth rate was fixed at about 5 Å/s monitored by a quartz crystal microbalance, and the substrates were kept at room temperature.

* To whom correspondence should be addressed. E-mail: liliang@issp.ac.cn.
† Chinese Academy of Science.
‡ Nanyang Technological University.
§ Chartered Semiconductor Manufacturing Limited.

10.1021/jp710230c CCC: $40.75
Published on Web 03/19/2008

The morphology of Al nanowires was characterized by field-emission scanning electron microscopy (FEI Sirion 200). The crystal structure was analyzed by X-ray diffraction (XRD, Philips PW 1700x with Cu κ_α radiation) and high-resolution transmission electron microscopy (HRTEM, JEOL 2010). In order to measure the thermal expansion of the Al nanowires, the high-resolution X-ray diffraction method was used with high-temperature attachments capable of controlling temperature within ± 1 K at the temperature range from 298 to 798 K. The X-ray diffraction data were collected by a step scanning method in the 2θ range from 30 to 70°. The X-ray diffraction patterns were obtained under high vacuum atmosphere at each stable constant temperature for about 15 min. For comparison, the lattice parameters of the Al thin films were measured at the same conditions. Field emission measurements were conducted in a vacuum chamber at a pressure of 4.6×10^{-8} Torr at room temperature. A rod-like aluminum probe with a cross section of 1 mm^2 was used as an anode and the Al nanowire array film served as a cathode. A dc voltage sweeping from 100 to 1100 V was applied to the sample.

3. Results and Discussion

Figure 1 shows the typical SEM images of Al nanowire array with different magnifications. It can be seen that large-area and ordered nanowire arrays are obtained. From Figure 1d, we can suggest the typical OAD deposition process. There is a large foreign particle on the Si substrate, behind which no nanowires are found. In this experiment, the vapor flux arrives at an oblique angle (87°) (shown in the direction of arrow) from the substrate normal and then the nanowires grow at an angle inclined toward the vapor source due to the atomic shadowing effect and surface diffusion, so the large particle blocks artificially the reach of vapor species and leaves an obvious empty area.

Figure 2a shows XRD pattern of the Al nanowire array. It indicates that the Al nanowires preserve a face-centered cubic (FCC) lattice structure as comparing with the standard diffraction of bulk Al. Figure 2b−c shows the typical HRTEM and SAED pattern of Al nanowires, which indicates that the Al nanowires are single crystals.

As a comparison to the nanowire samples, we also investigate the thermal expansion of Al films deposited at normal incidence using the same evaporation system. Figure 3a−b shows the SEM image and XRD pattern of Al films, respectively. It can be seen that the Al films are composed of many grains and grain boundaries, and have the same FCC lattice structure as Al nanowires.

Figure 4a shows three XRD patterns on Al nanowires measured at 298, 498, and 798 K, respectively. The diffraction patterns show no significant difference, except for the shift of peak position toward the lower angle direction with increasing temperature. From the X-ray diffraction patterns and Bragg equation, $2d\sin\theta = \lambda$ (d, θ, and λ are the interplanar spacing, diffraction angle, and X-ray incidence wavelength, respectively), the interplanar spacing can be obtained. For cubic structure Al, the lattice constant a can be calculated by the equation,

$$1/d^2 = (h^2 + k^2 + l^2)/a^2 \qquad (1)$$

where (hkl) and a are the crystal plane index and lattice constant, respectively. The variation of lattice constant of Al nanowires with temperature is shown in Figure 4b. After fitting the experimental data with the linear function, $a = a_0 + a_1T$, the obtained coefficients a_n can be used to calculate the thermal

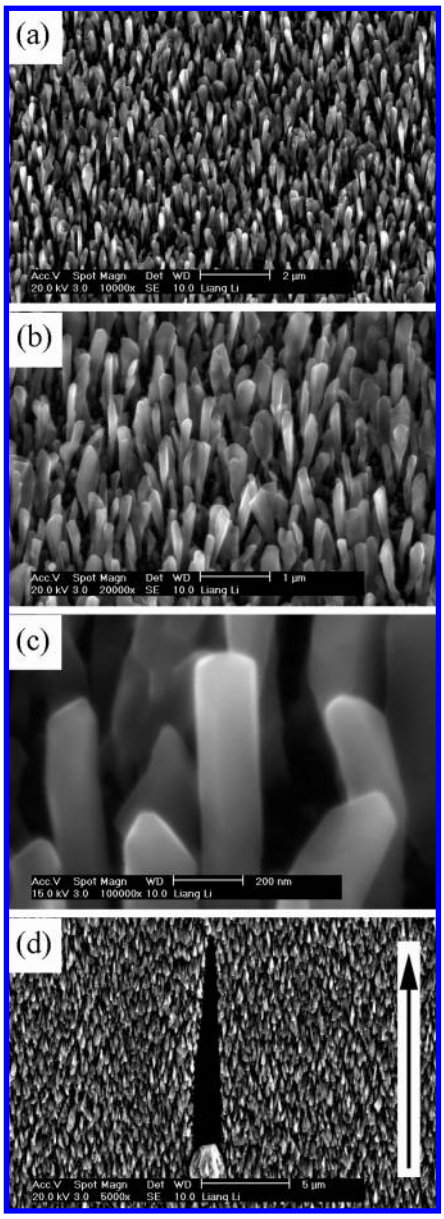

Figure 1. SEM images (a), (b), and (c) of the Al nanowires arrays at different magnifications. (d) SEM image showing a typical oblique angle deposition process.

expansion coefficient. The thermal expansion coefficient is defined as follows:[22]

$$\alpha = \frac{1}{a_0}\frac{\partial a}{\partial T} = \frac{a_1}{a_0} \qquad (2)$$

From Figure 4, the following results are obtained: (1) as-prepared Al nanowires have a smaller lattice constant 4.04517 Å than Al bulk 4.04924 Å and films 4.04918 Å; (2) the Al films have a larger thermal expansion coefficient than Al nanowires.

The as-prepared Al nanowires have a 0.1% smaller lattice constant than their equilibrium value of the bulk Al (111) peak. Compared with the bulk, the decreased or increased lattice constants have been observed in different nanomaterials. The intrinsic reasons are different depending on the fabrication technique and surface structure of the nanomaterials.[23−24] Here, we believe it is due to a tensile stress in the nanowire layer that reduces the lattice constant. The tensile stress may result from

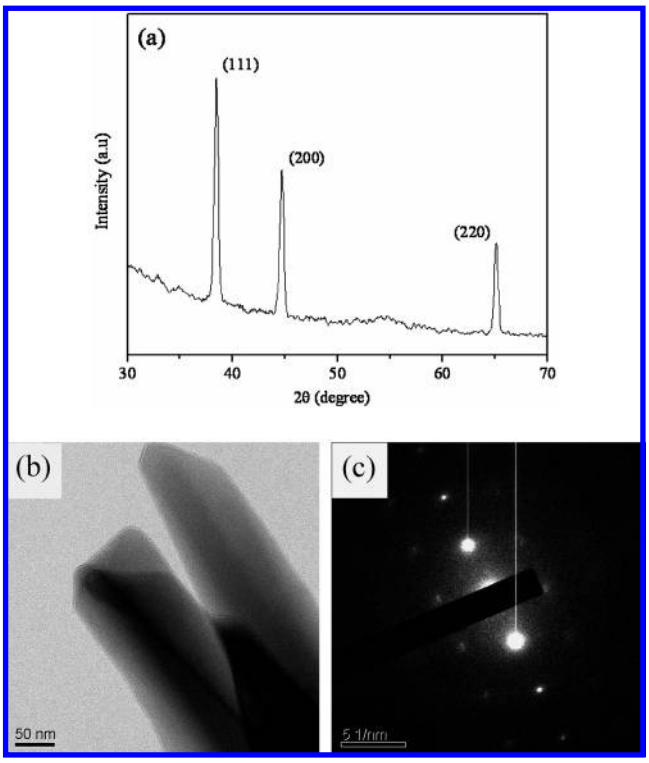

Figure 2. XRD pattern (a), HRTEM image (b), and SAED pattern (c) of the Al nanowires measured at room temperature.

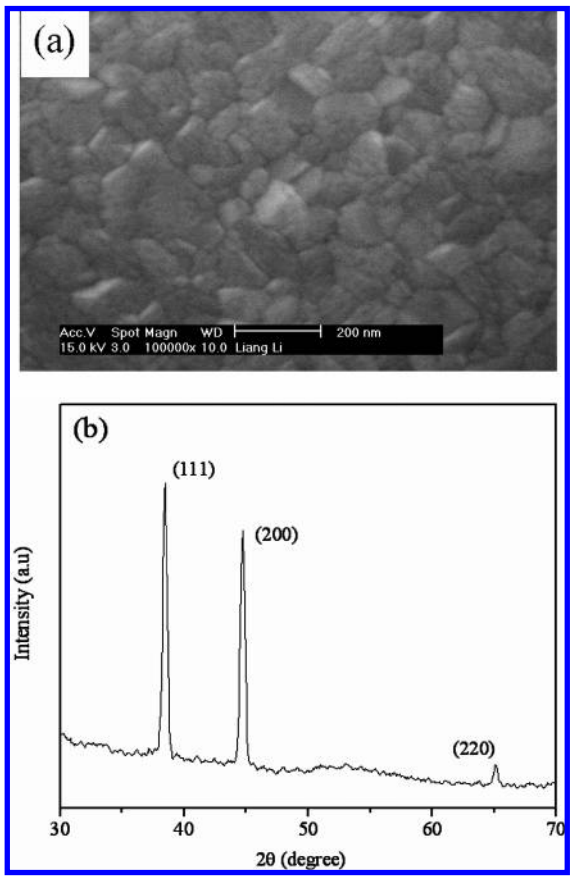

Figure 3. SEM image (a) and XRD pattern (b) of Al films.

the voids and defects associated with the shadowing effect during oblique angle deposition. In addition, the mismatch between thermal expansion coefficients of the substrate and the deposited materials usually also causes a stress. The as-deposited

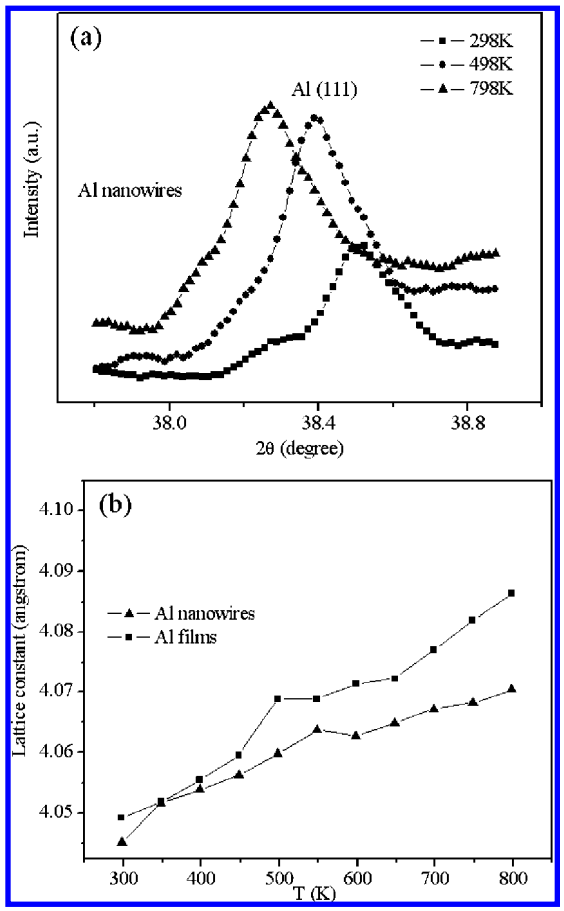

Figure 4. (a) XRD patterns of Al nanowires in situ measured at 298, 498, and 798 K, respectively; (b) temperature dependence of lattice constants of Al nanowires and Al films.

Al films correspond to a small tensile stress with a lattice constant of 4.04918 Å, which is 0.001% smaller than their equilibrium value. Compared with the Al films deposited at the same condition, the larger tensile stress in the Al nanowires further confirms that the stress in nanowires mainly originates from the voids formed during oblique angle deposition.

As we know, the thermal expansion behavior is determined mainly by the nonlinear vibration of crystal lattice, the more obvious the vibration, the larger the α. The contribution of nonlinear crystal lattice vibration in the grain boundary component is larger than that in the grain component because of disordered atomic arrangement in grain boundaries, which is due to the existence of many vacancies and vacancy clusters.[25] For Al films with a large volume fraction of grain boundaries, as show in Figure 3a, the nonlinear vibration of the crystal lattice becomes more obvious in both grain boundaries and grains with increasing temperature, which results in a large thermal expansion coefficient. For Al nanowires composed of a single crystal (Figure 2b), there are fewer grain boundaries with defects and vacancies compared with the Al bulk. In addition, with increasing temperature, the vacancies in nanowires would move more easily along the grain boundaries onto the surfaces of the nanowires and disappear quickly. As a result, atoms in grain boundaries may rapidly become ordered and make the nonlinear vibration contribution in grain boundaries to α decrease quickly, which causes the Al nanowires to have a small α.

Field emission measurements show that the Al nanowire arrays are potential field emitters. It is noted to date that there is not one paper devoted to the field emission of Al nanowires. Figure 5a shows the field emission current density *J* versus the

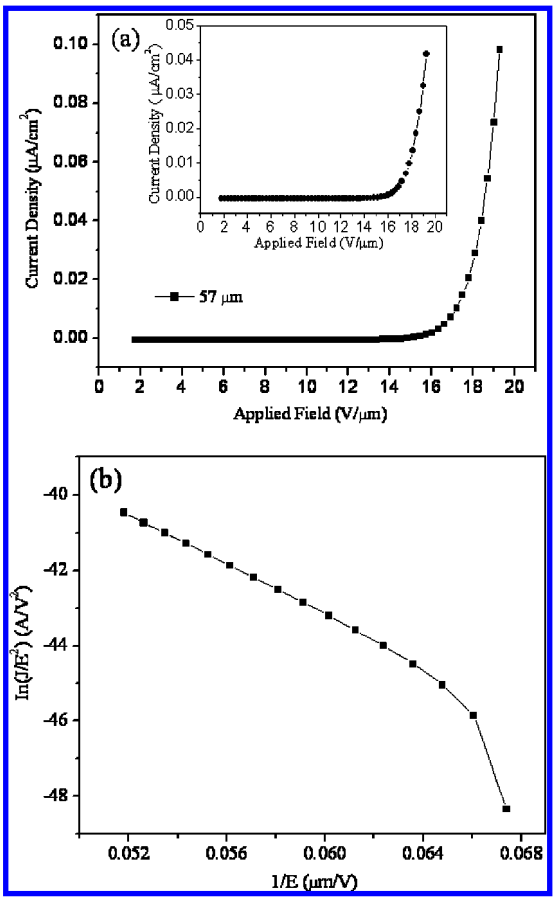

Figure 5. (a) Field emission current density J versus the applied field curve ($J-E$) for Al nanowire array with a distance 57 μm of between the electrodes (the inset is field emission curve of Al films); (b) corresponding $\ln(J/E^2)$ with $1/E$ F−N plot.

applied field curve ($J-E$) for Al nanowire array with a distance (d) 57 μm of between the electrodes. The turn-on field, defined as the applied filed to draw an emission current density of 10 nA/cm^2, is about 17 V/μm. For a comparison, we also measured the field emission performance of Al thin films under the same condition as nanowires. The corresponding turn-on voltage is about 18 V/μm, which is larger than the Al nanowire arrays (shown in the inset of Figure 5).

The FE current−voltage characteristics can be expressed by a simplified Fowler−Nordheim (FN) equation,[26]

$$J = (A\beta^2E^2/\phi)\exp(-B\phi^{3/2}/\beta E) \quad (3)$$

or,

$$\ln(J/E^2) = \ln(A\beta^2/\phi) - B\phi^{3/2}/\beta E \quad (4)$$

where $A = 1.54 \times 10^{-6}$ A eVV^{-2}, $B = 6.83 \times 10^3$ eV$^{-3/2}$Vμm^{-1}, β is the field-enhancement factor, and ϕ is the work function of the emitting materials, which is 4.28 for Al. The linear variation of $\ln(J/E^2)$ with $1/E$ (FN plot), as shown in Figure 5b, supports the hypothesis that the current is due to field emission, according to FN theory. From the slope of the linear part of the FN plot and using ϕ, β can be calculated to 176.2. β describes how the electric fields can be enhanced by protrusions from the emitting surface. Generally, β is related to emitter geometry (such as the aspect ratio), crystal structure, and the spatial distribution of emitting centers.[27] Here, the β value is not significant, but in future work, we try to improve it by the following methods: (1) optimizing the wire density by first patterning the substrate (templates) and then depositing nanowires on the preformed nanostructures such as nanodots with different densities; (2) increasing the aspect ratio of nanowires by prolonging the deposition time; (3) and utilizing the substrates with a good conductivity.

4. Conclusions

In summary, one-dimensional Al nanostructures were synthesized using a simple oblique angle deposition technique. The as-synthesized nanostructures were characterized using XRD, SEM, and HRTEM analysis. Compared with previous template methods, our synthesis method to create aligned Al nanostructures does not need templates, high growth temperatures or catalysts. So the intrinsic physical properties such as thermal expansion and field emission are studied more easily. In situ high-temperature X-ray diffraction results show that Al nanowires have a smaller thermal expansion coefficient than Al films, and field emission measurements indicate that the nanowires might be the potential candidates for cold field emitters after degrading the oxidation effect in the future.

Acknowledgment. The authors would like to acknowledge the support from the National Natural Science Foundation of China (No. 10704074), Special Project of Excellent Young Researchers of Anhui Province, and Support Project of Excellent President Scholarship of Chinese Academy of Sciences. L.L. would like to thank for the help of measurement and discussion from Dr. Xiaosheng Fang in Nanoscale Materials Center, National Institute for Materials Science, Tsukuba, Japan.

References and Notes

(1) Xia, Y.; Yang, P.; Sun, Y.; Wu, Y.; Mayers, B.; Gates, B.; Yin, Y.; Kim, F.; Yan, H. *Adv. Mater.* **2003**, *15*, 353.
(2) Li, L.; Yang, Y. W.; Li, G. H.; Zhang, L. D. *Small* **2006**, *2*, 548.
(3) Choi, J.; Sauer, G.; Nielsch, K.; Wehrspohn, R. B.; Gosele, U. *Chem. Mater.* **2003**, *15*, 776.
(4) Xu, X. J.; Fei, G. T.; Yu, W. H.; Zhang, L. D. *Appl. Phys. Lett.* **2006**, *89*, 181914.
(5) Cao, H. Q.; Wang, L. D.; Qiu, Y.; Zhang, L. *Nanotechnology* **2006**, *17*, 1736.
(6) Robbie, K.; Brett, M. J.; Broer, D. J. *Nature* **1999**, *399*, 764.
(7) Kennedy, S. R.; Brett, M. J.; Toader, O.; John, S. *Nano Lett.* **2001**, *2*, 59.
(8) Ye, D. X.; Karabacak, T.; Picu, R. C.; Wang, G. C.; Lu, T. M. *Nanotechnology* **2005**, *16*, 1717.
(9) Zhou, C. M.; Gall. D. *Appl. Phys. Lett.* **2006**, *88*, 203117.
(10) Singh, J. P.; Singh, J. P.; Liu, D. L.; Ye, D. X.; Picu, R. C.; Lu, T. M.; Wang, G. C. *Appl. Phys. Lett.* **2004**, *84*, 3657.
(11) Kennedy, S. R.; Brett, M. J.; Toader, O.; John, S. *Nano Lett.* **2001**, *2*, 59.
(12) Lee, Y. H.; Choi, C. H.; Jang, Y. T.; Kim, E. K.; Ju, B. K. *Appl. Phys. Lett.* **2002**, *81*, 745.
(13) Vila, L.; Vincent, P.; Dauginet-De Pra, L.; Pirio, G.; Minoux, E.; Gangloff, L.; Demoustier-Champagne, S.; Sarazin, N.; Ferain, E.; Legras, R.; Piraux, L.; Legagneux, P. *Nano Lett.* **2004**, *4*, 521.
(14) Davydov, D. N.; Sattari, P. A.; AlMawlawi, D.; Osika, A.; Haslett, T. L.; Moskovits, M. *J. Appl. Phys.* **1999**, *86*, 3983.
(15) Xu, X. J.; Fei, G. T.; Yu, W. H.; Chen, L.; Zhang, L. D. *Phys. Lett.* **2006**, *88*, 211902.
(16) Li, L.; Zhang, Y.; Yang, Y. W.; Huang, X. H.; Zhang, L. D. *Appl. Phys. Lett.* **2005**, *87*, 031912.
(17) Wang, Y. H.; Zhao, H.; Hu, Y.; Ye, C.; Zhang, L. *J. Cryst. Growth* **2007**, *305*, 8.
(18) Chang, M. T.; Chou, L. J.; Chueh, Y. L.; Lee, Y. C.; Hsieh, C. H.; Chen, C. D.; Lan, Y. W.; Chen, L. J. *Small* **2007**, *3*, 658.
(19) Zhou, J.; Ding, Y.; Deng, S. Z.; Gong, L.; Xu, N. S.; Wang, Z. L. *Adv. Mater.* **2000**, *17*, 2107.
(20) Fang, X. S.; Bando, Y.; Ye, C. H.; Golberg, D. *Chem. Comm.* **2007**, *29*, 3048.
(21) Ye, C.; Bando, Y.; Fang, X.; Shen, G.; Golberg, D. *J. Phys. Chem. C.* **2007**, *111*, 12673.

(22) Saotome, T.; Ohashi, K.; Sato, T.; Maeta, H.; Haruna, K.; Ono, F. *J. Phys.: Condens. Matter* **1998**, *10*, 1267.
(23) Qin, W.; Chen, Z. H.; Huang, P. Y.; Zhuang, Y. H. *J. Alloys Compd.* **2001**, *44*, 1915.
(24) Li, W. H.; Wu, S. Y.; Yang, C. C.; Lai, S. K.; Lee, K. C. *Phys. Rev. Lett.* **2002**, *89*, 135504.
(25) Wang, Y. H.; Yang, J. J.; Ye, C. H.; Fang, X. S.; Zhang, L. D. *Nanotechnology* **2004**, *15*, 1437.
(26) Shen, G.; Bando, Y.; Golberg, D. *Cryst. Growth. Des.* **2007**, *7*, 35.
(27) Wang, X. D.; Zhou, J.; Lao, C. S.; Song, J. H.; Xu, N. S.; Wang, Z. L. *Adv. Mater*. **2007**, *19*, 1627.